Optimisation of an Electric Bike

Group 16
Sub-system 1: Patrick Gonda, Sub-system 2: Colin Laganier, Sub-system 3: Hsinhua Lu
December 2020

Abstract

This report investigates the optimisation of a power assisted mountain bike (e-MTB). An e-MTB is a complex system with many elements to potentially optimise, but this study focuses on reducing weight of the bike by maximising performance per unit weight. The bike was split into 3 sub-systems: Drivetrain, Motor and Battery; these were chosen in context of there being 4 sub-systems, but the frame sub-system is excluded from this report and is to be assessed separately. The drivetrain is the cogs and chain that connect the motor to the rear wheel, and is chosen as a point of study as this element is mechanically complex. The motor must be efficient above all else, and has had very little development in use in bikes. Finally the battery is the heaviest part of the bike, so optimising this element is crucial. A blend of metamodeling and mathematical derivation was used to create each study to balance accuracy and feasibility. The tool used for optimization is the MATLAB Optimisation Toolbox, and each section used non-gradient based methods, with the drivetrain and motor additionally using gradient based methods. Post optimal analysis was done to verify the integrity of the results. The proposed solution is 2662g lighter compared to the unoptimized solution, which is a tangible reduction in weight for an e-MTB, and highlights the "evolutionary not revolutionary" style of bike development.

Figure 1: *Power assisted mountain bike.[1]*

1 Introduction

Power assisted mountain bikes offer both the ease of use of traditional bikes with the added power from an electric motor. However, a main issue with e-MTB is their heavy weight, which ultimately leads to lowered performance in terms of autonomy and thrust, as well as a less enjoyable experience for the rider. We are looking to optimise the overall weight of the bike. With the optimisation of the different parameters, it is expected that the main trade-off will be the price of the system, as the level of performance will be maintained. Another trade-off is that this optimization will tailor the different sub-systems to mountain biking and therefore the components will lose their flexibility and potential use in other systems.

2 System-level problem and Sub-system breakdown

The overall bike system can be divided in three distinct subsystems that can be independently optimised under a common objective of reducing the weight of the overall system.

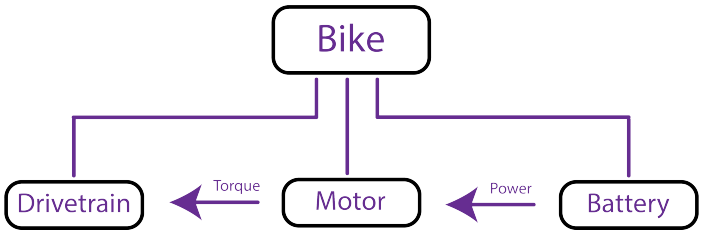

Figure 2: *System decomposition*

The power from the motor has to be moved to the rear wheel for the bike to move, and this is done through the drivetrain. This not only change the position of the motion but also the ratio between speed and torque. As an e-MTB is an all-terrain vehicle it is important that the range of gears is high enough for the bike to be able to overcome most gradients with the motor running at its most efficient. In addition, the battery performance could be hugely reliant on the motor, as nominal voltage and power-consumption are all interrelated. The systems will be first be optimized independently taking only few common parameters from industrial standards. Then the optimization results will be considered together to form a system-level three-dimension optimization solution, by giving the upper-bound of performance and subjective weights for each system.

$$\underset{\mathbf{x}}{\text{minimize}} \quad f(\mathbf{x}) = M_{drivetrain} + M_{motor} + M_{battery}$$

$$\mathbf{x} = n, \mathbf{s}, m, \mathbf{c}, N_a, P, r, W_m, Z, col, row, m, ch, co, d, t$$

3 Sub-system 1: Drivetrain

3.1 Optimisation Formulation

The force to move the bike will be generated by the motor in the frame to drive the rear wheel. The job of the drivetrain is to change this input to a suitable speed/torque to be used in different environments. The system is formed of two sets of cogs connected by a chain, which get shifted between each other with a derailleur. This section will focus on minimising the mass of the rear cassette ($\mathbf{s}$), front chainset ($\mathbf{c}$) and derailleur system by reducing the mass of each cog (s_i, c_i) and the amount of cogs (n, m). Whilst retaining the minimum range of gear ratios and maximum step size between each cog. The weight of each cog will be calculated though a simplified geometric metamodel, and all other limitations will be based on the current Shimano line-up of bike transmission components.

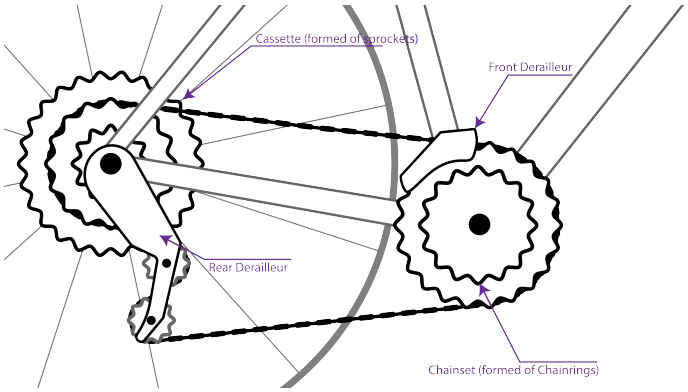

Figure 3: *Named elements of a Drivetrain.*

MTBs have historically had as many gears as possible, formed out of 8 sprockets in the back and 3 chainrings in the front (3x8). With racers requiring lighter bikes, 1x systems have become more popular, instead adding more gears in the back whilst removing the whole front system. With an e-MTB the work is done by a motor meaning comfort is no-longer a factor, so is a wide range of gears still necessary?

3.2 Model Development

Let us consider the following maximization problem:

$$
\begin{aligned}
\underset{n,\mathbf{s},m,\mathbf{c}}{\text{minimize}} \quad & t_w = \sum_{i=1}^{n} f_1(s_i) + \sum_{i=1}^{m} f_2(c_i) + f_3(n,m) \\
& f_1(s_i) = t * d(\frac{l^2 s_i^2}{4\pi} - \frac{s_h^2 \pi}{4})(1.1 - \frac{s_i}{100}) \\
& f_2(c_i) = t * d(\frac{l^2 c_i^2}{4\pi} - \frac{c_h^2 \pi}{4}) \\
& f_3(n,m) = a + f_4(n) + f_5(m) \\
& f_4(n) = b_1 \log(c_1 n - c_1 + 0.1) \\
& f_5(m) = b_2 \log(c_2 m - c_2 + 0.1) \\
\text{subject to} \quad & h_1(t) = t - 1.6 = 0 \\
& h_2(d) = d - 0.00805 = 0 \\
& h_3(l) = l - 12.7 = 0 \\
& h_4(s_h) = s_h - 32.5 = 0 \\
& h_5(c_h) = c_h - 64 = 0 \\
& h_6(a) = a - 210.4 = 0 \\
& h_7(b_1) = b_1 - 36.13 = 0 \\
& h_8(c_1) = c_1 - 316.0 = 0 \\
& h_9(b_2) = b_2 - 55.26 = 0 \\
& h_{10}(c_2) = c_2 - 9.124 = 0 \\
& g_1(n) = n - 12 \leq 0 \\
& g_2(n) = 1 - n \leq 0 \\
& g_3(m) = m - 3 \leq 0 \\
& g_4(m) = 1 - m \leq 0 \\
& g_5(s_i) = s_i - 53 \leq 0 \\
& g_6(s_i) = 10 - s_i \leq 0 \\
& g_7(c_i) = c_i - 57 \leq 0 \\
& g_8(c_i) = 10 - c_2 2 \leq 0 \\
& g_9(\mathbf{s},\mathbf{c}) = 4 - \frac{c_{max}/s_{min}}{c_{min}/s_{max}} \leq 0 \\
& g_{10}(s_i, s_{i+1}) = 0.78 - \frac{s_{i+1}}{s_i} \leq 0 \\
& g_{11}(c_i, c_{i+1}) = 0.78 - \frac{c_{i+1}}{c_i} \leq 0 \\
& g_{12}(s_i, s_{i+1}) = s_{i+1} - s_i \leq 0 \\
& g_{13}(c_i, c_{i+1}) = c_{i+1} - c_i \leq 0
\end{aligned}
$$

Constraints, simplification, and discretisation

The maximum number of gears and the size of the sprockets are all derived from values currently being produced by Shimano, these are from different line-ups due to specialisation, but there is no reason the mixed components would not work together. The chain will not be modelled in this scenario as the length of it is dependent on frame size.

All the variables in the problem space are integers, which would prevent the usage of gradient-based optimisation methods. To combat this the sprocket size will be modelled as a real value, and once the optimisation is complete the results will be discretised. The sizes of vectors S and C are non-constant, which most optimisers cannot work around, so the vectors will be the maximum size they can be, and then have redundant entries become zero.

Cog weight

The chainrings and sprockets are modelled with the circumference being calculated from the number of teeth multiplied by the distance between them. With the two dimensions defined calculating the mass is trivial from the assumed thickness and material density. For the rear sprockets cut-outs as illustrated below are often used to reduce the weight of the sprocket, and that is modelled as an increasing percentage decrease in mass. As the cut-outs are only used with large sprockets, it is assumed that the weight reduction from material removal is linearly dependant on the sprocket size, and that all the cogs are uniform in thickness.

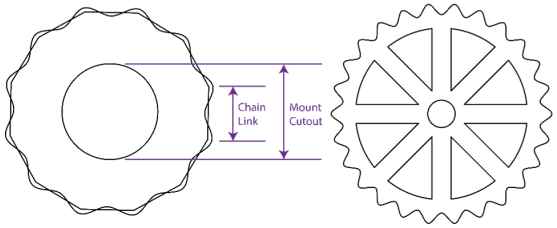

Figure 4: *representation of cog assumptions*

Derailleur weight

The weight of the derailleurs depends on the number of cogs in each set, but making this discrete would cause the optimisation to become non-gradient, and using a Fourier Series approximation would be computationally expensive, so a logarithmic function was fitted to the weights of the derailleurs. The function was centred at the point (1,0) to ensure that

Table 1: *Monotonicity Analysis*

	n	**s**	m	**c**		n	**s**	m	**c**
f	+	+	+	+	g_5		+		
f_1		+			g_6		-		
f_2				+	g_7				+
f_3	+		+		g_8				-
f_4	+				g_9		$> \Delta$		$> \Delta$
f_5			+		g_{10}		$< \Delta$		
g_1	+				g_{11}				$< \Delta$
g_2	-				g_{12}		$+/-$		
g_3			+		g_{13}				$+/-$
g_4			-						

the lack of a derailleur meant no additional mass, with a +0.1 offset applied to the function to prevent the asymptote from returning an undefined value. The mass used here is a sum of the derailleur and gear shifter found on the Shimano website.

3.3 Explore the problem space

Monotonicity analysis was done on the functions and constraints. The objective functions are increasing, and g_{1-7} are all upper and lower bounds of the input variables, with the upper bounds being potentially inactive as the optimiser is unlikely to reach the upper bounds of the problem. g_{9-11} either increase or decrease the range between each element, and this is properly bounded. Finally, g_{12-13} simply ensure the gears are sequentially decreasing in size. f_{1-5} are strongly increasing, so the objective function will also be strongly increasing, meaning optimisation should be feasible. Due to the non-constant vector sizes and advanced constraints optimising though algebraic methods is not possible.

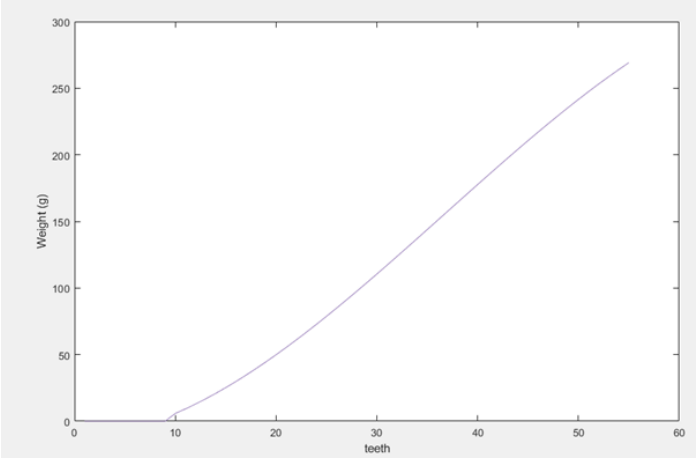

Figure 5: *Number of teeth in a sprocket against weight*

3.4 Optimisation

The tool used for optimisation is MATLAB, and 4 optimisers were used from the Global Optimisation Toolbox: Pattern Search, Genetic Algorithm (GA), Fminmax and Fmincon. Patternsearch is a non-gradient method which is very fast to converge, but the solutions were initially far from optimal as they were full of redundant sprockets, but after mesh refinement the solver would give very strong results. The initial issue was that the pattern search would start converging too fast and would fall into a local minimum. The next non-gradient method is GA, which generates multiple solutions, making the system more resistant to local minimum. This would produce sufficient results without major issues. The only quirk of this method would be the requirement of using a penalty system for the nonlinear constraints, as the algorithm would optimise outside of the constraints and then be unable to converge within the acceptable parameters due to the complexity of g_{9-13}.

The first gradient-based method used was Fminmax, as during model development it converged to feasible solutions more often than Fmincon, but once the model was completed it would fail to converge more often, and it was ultimately scrapped. Fmincon still struggles with local minima but it can be iterated to find the best starting position to find the global optimum. Each algorithm returned a different arrangement of gears, showing the increase in size of the rear gears necessary to compensate for range. Starting Fmincon at the solutions of the other solvers also yielded unusable results, which shows that those found are true minima.

Table 2: *Optimisation results against Shimano XT*

C#	PS	$\|PS\|$	GA	$\|GA\|$	FM	$\|FM\|$	XT
S1	24.3	24	33.8	34	43.8	44	45
2	19.0	19	26.3	26	34.2	34	40
3	14.8	15	20.5	21	26.7	27	36
4	11.5	12	16.0	16	20.8	20	32
5	10.0	10	12.4	13	16.3	16	28
6	10.0		10.0	10	12.8	13	24
7	10.0		10.0		10	10	21
8	10.0		10.0		9.3		18
9	10.0		10.0		9.3		16
10	10.0		9.8		9.2		14
11	9.5		9.6		9.1		12
12	9.0		9.1		9.1		10
C1	38.4	38	26.0	26	22.0	22	28
2	30.0	30	22.0	22	21.3		
3	21.4		21.2		21.3		
t_w(g)	110	1102	1034	1038	932	929	1463

3.5 Discussion

The final output of the optimisation proposes a 1x7 configuration weighing 930g, which is significantly lighter and has less gears than the existing solution (1463g), so an e-MTB can shed a significant amount of weight by removing redundant gears. The lower largest sprocket (44/45) still has a suitable range, and the smaller front sprocket (22/28) is not a concern as the motor can still generate enough torque to move the bike. This sub-system was a challenge to optimise due to the large number of variables and local minima, meaning the starting point would heavily affect final convergence and finally parallel computing was used to speed up the process. Gradient-based methods specifically struggled with this problem as it is non-convex, and had the problem space been simplified further such as focusing only on the rear cassette gradient-based methods could have been more appropriate. The final results for the non-gradient methods were generated within seconds, as compared to 10s of minutes for Fmincon iterated through a set of starting values. The non-gradient methods use random decision-making at times, meaning that the results would differ after every run, and these best results are listed above.

The model is an accurate representation for the goal of optimising the system for weight, but the objective value has limited use outside of being a comparison as the fundamental weights are meta-models. Using more accurate models would exacerbate the existing issues with convergence and speed, so the current method is the best.

4 Sub-system 2: DC Motor

Brushless DC motors are most commonly used in electric bikes, due to their efficiency and high torque. For this research, the stator of an outrunner permanent magnet brushless DC motor will be studied. The stator is an electromagnet, with a set number of teeth, each with a copper coil winding that is periodically charged. The rotor is the rotating hub and shaft, fitted with a set number of permanent magnets (or poles). The profile of the DC motor is highly customisable due to the large number of parameters. Those studied in this subsection are: the number of coil windings (N_a), the number of rotor poles (P), the radius of the stator (r), the thickness of the stator (W_m) and the number of stator teeth (Z). As the power and weight are the most crucial elements of the bikes, the torque to stator weight ratio will be optimised.[2]

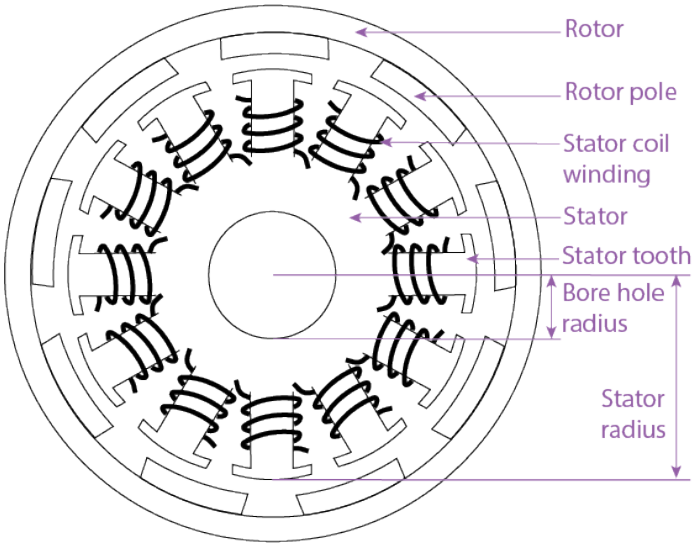

Figure 6: *Diagram of the motor's rotor and stator*

4.1 Optimisation Formulation

Let us consider the following minimisation problem:

$$
\begin{aligned}
\underset{N_a, P, r, W_m, Z}{\text{minimize}} \quad & f = \frac{-T(N_a, P, r, W_m, Z)}{M_{motor}(N_a, r, W_m, Z)} \\
& T = \frac{P N_a F_{pp} I}{2\pi A} \\
& F_{pp} = \frac{2 B_m 2 r W_m}{Z} \\
& B_m = \frac{B_r}{\pi}[atan(\frac{L_m W_m}{2z\sqrt{4z^2 + L_m^2 + W_m^2}}) - \\
& atan(\frac{L_m W_m}{2(D_m + z)\sqrt{4(D_m + z)^2 + L_m^2 + W_m^2}})] \\
& M = M_s + M_w \\
& M_s = D_s W_m (\frac{\pi r^2}{2} - \pi r_b^2 + \\
& Z(\frac{2\pi\alpha r}{Z}\frac{r - W_t}{4} + \frac{2\pi r W_t \beta}{2}) \\
& M_w = Z N_a \pi D_w r_w^2 (2(0.001 + \frac{2\pi\alpha r}{Z}) + \\
& 2(0.001 + W_m)) \\
\text{subject to} \quad & g_1(N_a) = N_a - 60 \leq 0 \\
& g_2(N_a) = 1 - N_a \leq 0 \\
& g_3(P) = P - 23 \leq 0 \\
& g_4(P) = 2 - P \leq 0 \\
& g_5(r) = r - 0.05 \leq 0 \\
& g_6(r) = 0.015 - r \leq 0 \\
& g_7(W_m) = W_m - 0.08 \leq 0 \\
& g_8(W_m) = 0.01 - W_m \leq 0 \\
& g_9(Z) = Z - 24 \leq 0 \\
& g_{10}(Z) = 3 - Z \leq 0 \\
& g_{11}(P, Z) = P - (Z - 1) \leq 0 \\
& g_{12}(N_a, r, Z) = \\
& \left\lfloor \frac{N_a}{1000(\frac{r(\beta - \alpha))}{4})} \right\rfloor - (\frac{1000\alpha\pi r}{Z}) \leq 0 \\
& g_{13}(N_a, P, r, W_m, Z) = 2 - T \leq 0 \\
& g_{14}(N_a, r, W_m, Z) = M_{motor} - 1.5 \leq 0
\end{aligned}
$$

4.2 Model Development

Torque

The equation of the torque of the DC motor was derived from the formula of the Counter Electromotive Force (CEF) [3]. The torque is generated by rotational motion caused by the electromagnetic attraction of the charged stator conductors and the rotor poles. To calculate the torque of the different combination of parameters, the coil current (I) was set to 15A, which is a standard for most motors used in applications like electric bikes, while the number of path (A) was set to 2, as a wave winding pattern is most commonly used in these types of DC motors due to its high efficiency [3]. To calculate the Flux per pole (F_{pp}), the average flux density of the permanent magnets was multiplied by the area of the stator teeth it will interact with. Finally, the flux density (B_m) was calculated using a typical Neodymium magnet (NdFeB N35), simplified to a rectangular cuboid [4]. It's residual magnetism (B_r) was identified from its material properties [5], while the most commonly used magnet thickness (D_m) of 2.5mm was used [6] and the rotor-stator airgap (z) was set to 2mm as it was identified to be a common size which would not affect the motor negatively. Finally, the magnet's dimensions were set to be the maximum possible while ensuring equal adequate spacing in between each of them.

Mass

The mass equation used for the optimisation takes into account both the weight of the stator body, as well as the weight of the coil winding used. To calculate the mass of the stator, a simplified formula of its volume was created. This simplification removes all fillets, but overall represents an accurate approximation of the volume, which can be multiplied by the density of the laminated steel (D_s) used. The radius of the center bore hole (r_b) was set to 1.25mm, a standard for most stators of this size. The width and end-width of each tool were respectively defined as 40% and 80% of the available tooth width based on research studying the efficiency of DC motors [7]. Finally, the mass of the coil winding was simply calculated from the dimensions of the stator tooth and the number of windings variable and multiplying that by its density. The layering of the coil was not taken into account in the mass calculations a the thickness of the coil was very small (1mm) and therefore would not have had an important influence on the overall weight.

Constraints

The minimum and maximum number of rotor poles and stator teeth were established from what is commonly available within our dimensional constraints on the market. The bounds of the stator radius and thickness were both deter-

Table 3: *Monotonicity Analysis*

	N_a	P	r	W_m	Z		N_a	P	r	W_m	Z
T	+	+			-	g_5			+		
F_{pp}	+	+			-	g_6			-		
B_m						g_7				+	
M_s			+	+	+	g_8				-	
M_w	+		+	+	+	g_9					+
M_{motor}	+		+	+	+	g_{10}					-
g_1	+					g_{11}		+			-
g_2	-					g_{12}	+		-		
g_3		+				g_{13}	-	-	-	-	-
g_4		-				g_{14}	+		+	+	+

Table 4: *Results of different optimisation algorithms*

Algorithm	N_a	P	r	W_m	Z	T	W	T/W
Interior-point	54	2	32	11	3	2.0	0.31	6.52
Active-set	60	4	36	10	5	2.9	0.43	6.73
SQP	18	4	27	76	5	2.1	1.3	1.63
GA	36	12	48	10	13	2.9	0.86	3.36
GAmultiobj	32	9	42	25	10	3.7	1.4	2.59
Paretosearch	56	6	50	22	7	5.7	1.5	3.69

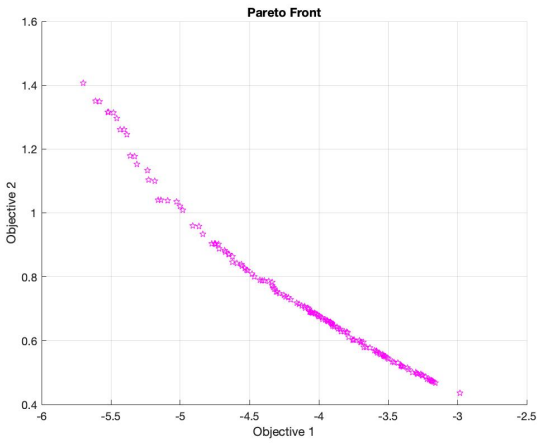

Figure 7: *Pareto Front of Pattern Search*

mined from the dimensional constraints of a mid-drive electric bike. Finally, the bounds of the number of coil windings was semi-arbitrarily setup from research into case-studies, as additional constraints were created for this variable. The first additional inequality constraint ensures that the number of rotor poles is strictly less than the number of stator teeth. This is an important constraint for the smoothness of the DC motor, as it was shown that this reduces the vibrations created when in use. The second additional constraint ensures that the thickness of the overlaid coils in the winding does not exceed the end width of the stator tooth. As some of the variables were discrete while the others were continuous, it was decided to simply round the optimised discrete parameters to the nearest whole number at the end.

4.3 Explore the problem space

A monotonicity analysis was undertaken to study the functions and constraints of the sub-system. Both the torque and mass function are both increasing, and therefore objective function is decreasing. The constraints g_{1-10} are the upper and lower bounds of the variables. Some of these will be inactive, as the lower bound of increasing functions will never be used by the solver. Due to the complexity of the problem and the uncertainty around certain constraints, even those suspected of being partially inactive were kept.

4.4 Optimisation

The optimisation of the DC motor was done using MATLAB and 4 prebuilt solvers from the Global Optimisation Toolbox. Firstly, a gradient-based constrained optimization was done using the Fmincon solver with three different algorithm: interior-point, active-set and SQP. However, these first attempts struggled to optimise the sub-system and would not yield a global minimum. This was overcome by adding new constraints and slightly modifying the objective function. To further tackle the local minimum issues faced when using the previous solver, direct search algorithms were used to further optimise the sub-system. Firstly, a Genetic Algorithm solver was used to optimise the sub-system. This method offered generally positive results, however would occasionally run into the problem of finding values that would not meet the constraints established and therefore fail to output a result. Secondly, as the objective function was a ratio, it could be separated into a multi-objective function, separating the torque and the weight. By using the GAmultiObj solver, with random initial values and both functions, a Pareto set was obtained. Finally, by doing a preamble optimisation of both functions using Fmincon, and setting those values as the initial points for a Pattern Search, a final Pareto set was created. For both of these Pareto sets, the values were normalised and a maximal ratio was returned with the optimal values identified. The results from each solver can be seen in Table 4.

4.5 Discussion

By conducting research on the torque produced by typical electric bike motors [8], it was found that 60Nm was the average torque offered by most units. Additionally, the gearbox ratio used with these motors ranged from 20:1 to 40:1 [9]. It was decided that a 30:1 gearbox would be reasonable and that therefore adding a minimum torque constraint of 2Nm would enable the optimisation to create a more guided result. The weight of stators of larger DC motors like the one optimised is not available online, however, it was found that the stator represents about a third of the overall weight of the motor unit. From market research, the typical weight of the motor units ranges from 3.5 to 5kg, and therefore any stator under 1.5kg would be an improvement.

As the optimisation was minimising a negative ratio, many different configurations can seem optimal and statistically are clear improvements from random parameters. The Genetics Algorithms used would return a different value with every run, and therefore are difficult to draw conclusions from. Regarding the multi-objective optimisation, while the Pareto Front offers a general idea of the trade-offs and advantages that can be achieved, no real conclusions can be drawn. By adding more design features or requirements, such as the cost or a constraint of a certain parameter, a better conclusion could be drawn.

The setup with the highest torque to weight ratio was obtained by the Fmincon solver with the Active-set algorithm, it also is the second lightest configuration, weighing only 426g (a 1074g reduction) and outputting a theoretical torque of 87Nm after the gear reduction. Further optimisation of the sub-system may also entail the development of functions to take into account the Copper, Iron and Mechanical losses depending on the stator configuration. However, the theoretical calculation are quite complex and would require the modelisation of the rotor and shaft as well [10].

5 Sub-system 3: Battery

5.1 Optimisation Formulation

Theoretical approach

E-bike battery is modelled as a compound structured lithium battery with three sub-model, where they are interrelated through performance level and dimension. Lithium model is chosen for its relatively high energy density and low cost, which is desirable for EV application [11].

A. battery cell sub-model ($\mathbf{M}_{cell}$)

18650 and 21700 models are chosen as battery cell sample, where 34 type of most used cells in EV industry are selected from the market from capacity of 1100 to 5000 mAh [12][13].These cell models are known for their high energy density, small size and efficiency, which perfectly match the goal. Each battery cell is modelled as a capacitor and a resistor in parallel and connected in serial or parallel in group as shown in Figure 6.

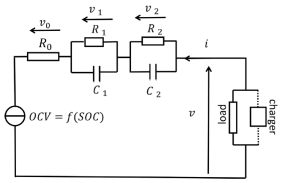

Figure 8: *Battery equivalent circuit*

B. equivalent circuit sub-model (ECM) ($\mathbf{P}_{index}$)

The battery ECM is given in Figure 6, where the open-circuit-voltage(OCV) is depending on the state of charge by z(t). As the OCV hysteresis is low and therefore negligible, the model is simplified to a Thevenin circuit [14]. Then, performance property of whole battery could be inferred and used for evaluation.

C. physical sub-model ($\mathbf{M}_{pipe}, M_{case}$)

The physical sub model consists of protection casing (with battery controller) and cooling pipe. To ensure the battery performance, Tesla patent cooling tube is considered and hugely simplified to minimized weight as shown in Figure 7 [15]. In addition, all the battery in column are connected in parallel while the one in row are in series to save space for controller circuit at top. Therefore, based on all sub-models, the dimension and the mass of the case and whole battery could be calculated given fixed thickness.

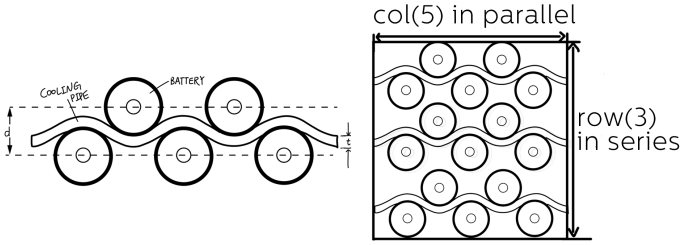

Figure 9: *Battery arrangement example*

D. model and parameter assumptions

All sub-models are simplified with following assumptions:

1. Same type of batteries used are considered identical, and functional failure does not occurred. The efficiency of whole battery is constant and set at 74%.[16]
2. The internal Resistant and OCV of whole system is neglected. And so that, performance is not effected by external factors such as working temperature or SOC, etc.[17]
3. Manufacture tolerance of case and pipe is neglected.
4. The material used are isotropic and uniform in density, and the parameters in nomenclature are assumed to be constant.

Variables and constraints

The cell layout comprised of number of cells in row and column is taken as design variable. Besides, the type number of cell is also considered where it is corelated with the performance property of single cell. This includes mass(m/g), maximum discharge current(ch/A), capacity (c/mAh) and cost(co/$). Distance(d/mm) and thickness(t/mm) shown in figure 7 are also considered.
Constraint are made and explained as below:

$$
\begin{aligned}
g_1 &= 7 - row \le 0 & g_8 &= ch - 38 \le 0 \\
g_2 &= row - 30 \le 0 & g_9 &= 2 - co \le 0 \\
g_3 &= 39 - m \le 0 & g_{10} &= co - 2 \le 0 \\
g_4 &= m - 75 \le 0 & g_{11} &= 2.5 - t \le 0 \\
g_5 &= 17.5 - d \le 0 & g_{12} &= t - 7.5 \le 0 \\
g_6 &= d - 22.5 \le 0 & g_{13} &= col - row \le 0 \\
g_7 &= 4 - ch \le 0 & g_9 &= 3.6row - 36 \le 0 \\
g_{14} &= -c * col + 10000 \le 0 \\
g_{15} &= 15row + row * t - 250 \le 0 \\
g_{16} &= -18.3\text{col} + 200 \le 0
\end{aligned}
$$

Table 5: *Constraints explanation*

g	explanation
$g_{1:2,13}$	Industrial standard of arranging cells [18]
$g_{3:12}$	The range given by all 34 type of 18600 and 21700 battery in the market.[19]
g_{15}	Minimum capacity for mountain bike standard battery
$g_{16,17}$	To fit in the normal e-bike frame in market[20]

Model formulation

Based on the submodels, the problem is formulated as following formula, where detailed simulation is run in python:

$$
\begin{aligned}
M_{total} = M_{cell}(col, row, m, ch, co) + M_{pipe}(col, row, d, t) \\
+ M_{case}(col, row, d, t)
\end{aligned}
$$

5.2 Model Development

Design space sampling

Due to the complexity of the models, a design of experiment (DoE) was implemented to thoroughly fulfil the multiple objectives. Fractional factorial sampling was chosen initially as it could include all battery type and electronic circuit layout. However, due to the slow run time n^d , Latin hypercube was chosen instead to sample continuous d and t. Lastly, a and Gaussian distribution sampling algorithm is coded based on pseudo code of Metropolis-Hasting. This help to sample the discrete number of rol and col without selection bias, while excluding the large potential noise set

of irregular shape. Noise set was identified using g_{16} and g_{17}. This sampling process hugely improve the validity of the objective function within rigorous constraints of mountain bike. The sampled points were then combined using full factorial approach. This DoE gathers data of the battery weight and performance against design variables for each sampled points by conducting simulation model designed in 5.1.

Ideal Performance Index

The second objective function is also generated as below:

$$P_{index} = 1.5P_{capacity} + 0.8P_{cost} + 0.2P_{charge} + 0.4P_{heat} + P_{voltage}$$

Model selection

To produce the surrogate model, four options are considered, linear regression(LR) with polynomial feature, Neural network, Krigging and Polynomial Response Surface (PRS). Krigging interpolate values governed by covariances between test set and measured set. However, it works better for isotropic data without trend. Neural network apply Universal approximation Theorem for continuous dataset, but could be easily overfitted with large number of variable and limited parameter. LR work similarly to polyfitn function based on PRS. However, due to large size of dataset in which battery type is hot-encoded, linear regression works more efficiently. This is because LR synergize with the backward elimination, which is considered crucial in this case of 34 terms. In addition, due to the potential noise set generated by full factorial sampling and relatively weak learning ability of LR, an ensemble learning was made with bootstrap aggregation. This reduce overfitting and undesirable influence of noisy samples while aggregating the predictions to select best prediction.[21]

Model construction

To construct the ensemble learning, battery type is hot-encoded to eliminate numerical influence in categorical data. However, the result is undesirable as 34 additional Boolean variable could cause huge number of local minimum which is unfavorable for optimization especially for gradient-based model. Besides, problems could occur when working with polynomial features where 741 terms are generated. Model overfits easily and doesn't fit to the theoretical model and cross-validation. Therefore, cell properties are taken as independent variable which add up the variable number to 8. An autonomous backward elimination algorithm was designed based on the adjusted R2 (0.05 as boundary). And the model work well with bagging regression in ensemble.

Model testing

Three method of validation is made to evaluate and adjust the model. Firstly, cross validation of test set is made where mean squared log errors(MSLE) were compared between degree 1 and degree 2 polynomial feature models. MSLE is chosen because the result is large where percentage error could demonstrate more accurately. In addition, the objective function is high degree polynomial, in which MSLE could lower the dominance of high degree errors. As shown in the table, and predicted in theoretical model, result is best fit to degree 2 function. Then, the accuracy of model is then evaluated by adjust R2 to find the relevance of each terms. As the result, LR with backward elimination choose the influential terms successfully. Lastly, sample reweighting is done to ensure the objective function is accurately fit to the regular-shape sample points (real-life battery dimension) and learn deeply the hard samples, without overfitting

Table 6: *MSLE for different degree approach*

Degree 1	Degree 2	Interaction only	Degree 3
2.3e-3	1.84e-6	1.628e-5	9.84e-5

Table 7: *Adj R2 for hot-encoded and backward elimination approach*

LR(hotencoded)	LR(BE hotencode)	LR	LR(BE)
2.3e-3	1.84e-6	1.628e-5	9.84e-5

to the noisy samples. This test provide confidence to the result while prove validity of the MH sampling for the row and col number.

5.3 Explore the problem space

The full derivation of two objective function on mass and performance index could be found **here** as it was lengthy. As for the constraint, they were already shown in 5.1. Monotonicity analysis was conducted and shown together with the objective function. g_{17} was eliminated based on regional monotonicity as it is dominated by g_{13} and g_1.

5.4 Optimisation

Optimization method selection

The optimization is implemented using stochastic non-gradient-based methods, genetic algorithm(GA) and paretosearch algorithm(PA). GA uses huge search space and generations to find global minima, whereas PA uses pattern search iteratively for non-dominated points. Due to the few variables involved, possibility for objective function to be convex, and the existence of local minima, these two algorithm are chosen. In addition, as multi-objection optimization is subjected to bounding and smooth inequality constraint, PA and GA should be able to perform well. Then, a fmincon algorithm with sequential quadratic programming(SQP) solver is run to set starting point for PA and GA. SQP converges to the optimum by tightening the feasibility of the optimisation constraints[22]. Compared to other solution, like interior-point algorithm, it generates more accurate and natural result despite large memory usage and computational complexity.

GA/PA result

The four result from GA and PA, setting starting point or not are showed in figure 8.

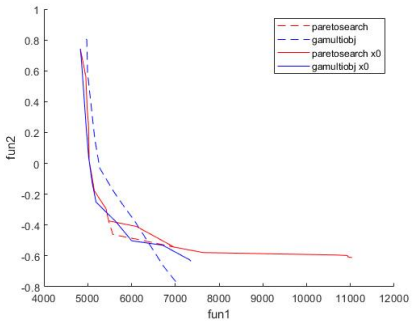

Figure 10: *constraint explanation*

After adding initial point, GA improves hugely as it lean toward the origin, whereas PA remains unchanged. With larger dataset, the dependency on the starting point was reduced, however, GA still perform better than PS as its high

Table 8: *Spread measure and average distance of solutions from different approach improving GA*

	MSG	FT	Hybrid fgoal	GA re-run
Avg.dis	3.1e-2	2.2e-2	2.4e-2	1.3e-2
spread	0.0866	0.1734	0.0934	0.4199

adaptability in large search space. When considering diversity, it is significantly crucial as the final result should correspond back to discrete battery property in which less pareto front solution may lead to no suitable battery type. GA approach was considered less desirable as it produce 'elite set' of result with the Pareto front solution number of 11 much less than 30 in PA. Therefore, little tweak is given to GA for better diversity while maintaining better fitness value(rank).

Improved GA

First, a distance measure function is added in design space (genotype). This measure is set to encourage the evolution of subsets representing diverse solution in a single population during the evolutionary process.[23] This function could also be used to evaluate following tweaks on GA. In addition, pareto fraction, function tolerance(FT) and maxstallgeneration(MSG) are also increased in GA to further diversify the result. Then a hybrid option of fgaolattain based on SQP is added to the GA. It results a optimal Pareto front, despite losing diversity. However, it allows designer to have relatively imprecise goal, in my case, the exact boundary for final result to be diverse enough to relate back to specific battery. Therefore, in order to regain diversity, with final population returned last run, GA is run again removing the hybrid function. The results are given in Table 6.

Post optimal analysis

The parametric study is done by reran all of the model from the previous section with changed parameters. The large difference in the solutions compared to previous one show that the design variable is highly dependent on calculation of performance index, as different type of battery should be selected for different requirement.

5.5 Discussion

In the optimization process, GA and PA perform accurately and efficiently compared to SQP which is hugely effected by local minima. However, SQP is then used to set initial condition for GA and PA to improve the accuracy while hugely relieve the computational stress. According to Figure 9, GA overall is smooth and better rat fitness value. On contrary, PA exhibited fluctuations and tend to be straight at most of the sample points, which indicates space for improvement when evaluated by theoretical model in 5.1. However, this optimization formulation could be improved by writing a new algorithm to iterate through and choose best initial guess for PA. In this case, hybrid algorithm with PA could also be tested. This is because theoretically hybrid function with pattern search is capable to solve non-smooth region near the solution. Further, the tweaking of GA could be iterated through different combination of option, especially on the stopping criteria of max_generation and function_tolearance. Fgoalattain could also be compared with other hybrid method. Overall, the main challenge in this study is to fit both the objective function and optimization model toward the discrete dataset produced by categorical data, and try to avoid the large inevitable noise set produce in the sampling phase. However, model testing result showed that the problem was solved successfully with MH

Table 9: *Spread measure and average distance of solutions from different approach improving GA*

col	row	battery	d	t
9	10	INR21700-50E	17.505	2.514

Table 10: *Final difference in weight*

	Drivetrain	Motor	Battery	Total
Starting weight(g)	1463	1500	6000	8963
Optimal Weight(g)	929	426	4942	6297

sampling, backward elimination and hybrid function. Lastly the pareto set was brought back to correspond to specific battery cell model. Subjective weighted objectives and RMS error between desirable property of cell and specific model were calculated and compared. The final result is showed in Table 7.

6 System-level discussion

The drivetrain optimised by Fmincon weighs 929g as opposed to 1463g of the standard drivetrain, showing that if a e-MTB specific drivetrain is to be used the bike would be significantly lighter, whilst retaining the range and step size necessary for operation. Compared to the other sub-systems this brings a significant but not exceptional improvement to weight.

The DC motor stator optimised by Fmincon weighs 426g opposed to the 1500g estimated standard e-MTB stator. Additionally, the torque produced by this DC motor after gear-reduction reaches 87Nm, therefore far greater than the goal of 60Nm, and greater than most motors available on the market today. This is a significant weight reduction and a positive torque increase for the system as a whole.

The battery is optimized by a muti-objective hybrid model of Genetic algorithm and fgoalattain. The final weight is reduced to 4942g from 6000g for a normal mountain bike battery, while the performance matrix is maintained at a level slightly higher than the average. Additionally as the battery is closely related to the motor sub-system, the optimization of the battery model should take the optimal voltage and power usage from the result into consideration. But in reality this process should also consider the flexibility for the battery to be assembled on different e-MTB designs, and weighed together to generate a final multi-objective function.

7 Conclusion

The drivetrain optimisation successfully highlighted redundancies in the current drivetrain style. The motor optimisation creates a new combination of parameters to produce the required torque with a lower weight. The battery optimisation found a unique way to minimize a weight by changing the battery cell layout and combined with cooling pipe and battery control circuit. The shape tend to be closer to a square, which is quite different from most of the long and thin e-MTB batteries on the market. However, in the mountain e-MTB case, this design perfectly fit the requirement of reducing the weight while remain performance at certain level. The proposed solution is 2662g lighter compared to the solution, which is a tangible reduction in weight for an e-MTB, and highlights the "evolutionary not revolutionary" style of bike development.

8 Nomenclature

8.1 Sub-system 1: Drive-train

Var	Value	Units
t_w	Drive-train weight	g
n	Number of sprockets	n/a
$\mathbf{s}$	Number of teeth in each sprocket	n/a Vector
m	Number of chainrings	n/a
$\mathbf{c}$	Number of teeth in each chainring	n/a Vector

Cst	Value	Source	Units
t	Thickness of cogs	[24]	mm
d	Density of cogs	[25]	g/mm^3
l	Length of each cog tooth	[24]	mm
s_h	Cutout diameter sprockets	[26]	mm
c_h	Cutout diameter chainrings	[27]	mm
a	Value in derailleur model	Derived	n/a
b_1	Value in derailleur model	Derived	n/a
c_1	Value in derailleur model	Derived	n/a
b_2	Value in derailleur model	Derived	n/a
c_2	Value in derailleur model	Derived	n/a

8.2 Sub-system 2: DC Motor

Var	Value	Units
f	Torque to weight ratio	Nm/kg
N_a	Number of coil windings	n/a
P	Number of rotor poles	n/a
r	Radius of stator	m
W_m	Thickness of stator	m
Z	Number of stator teeth	n/a

Cst	Value	Source	Units
A	Number of parallel paths	[3]	n/a
α	Stator tooth width factor	[7]	n/a
B_r	Residual magnetism of NdFeB N35	[5]	T
β	Stator tooth end width factor	[7]	n/a
D_m	Rotor magnet thickness	[6]	m
D_s	Density of laminated steel	[28]	kg/m^3
D_w	Density of copper coil	[29]	kg/m^3
I	Armature current	[30]	A
r_b	Stator bore hole radius	Derived	m
r_w	Thickness of 18AWG copper coil	[31]	m
W_t	Stator tooth end thickness	[7]	m
z	Rotor-stator gap	[3]	m

8.3 Sub-system 3: Battery

Var	Value	Units
col	Number of cells in column (parallel)	n/a
row	Number of cells in row (series)	n/a
$cost$	Cost of single cell	$
m	Mass of single cell	g
c	Capacity of single cell	mAh
t	thickness of cooling pipe	mm
ch	maximum discharge current of single cell	A
d	vertical distance between battery in same row	mm

Cst	Value	Source	Units
t_c	Thickness of case	[18]	mm
d_{ABS}	Density of ABS	[32]	g/mm^3
d_{al}	Density of Aluminum alloy 6060	[33]	g/mm^3
s_h	Efficiency of battery	[14]	n/a
c_{imb}	capacity imbalance	[14]	n/a
C_{total}	Total capacity of battery	Derived	mAh
OCV	Open circuit voltage	Derived	V
h_{cell}	Height of single 18650 and 21600 cell	Derived	mm
d_{cell}	Diameter of single 18650 and 21600 cell	Derived	mm

References

[1] AMB Magazine. Tested: Bosch performance line cx e-mtb mode, 2017 Accessed 11/2020. https://www.ambmag.com.au/feature/tested-bosch-performance-line-cx-e-mtb-mode-472988.

[2] MIT Edgerton Center. Case study: Razor scooter wheel motor, 2009 Accessed 11/2020. http://web.mit.edu/first/scooter/motormath.pdf.

[3] Sheppard Joel Salon. 4 - introduction to electric machines. In WAI-KAI CHEN, editor, *The Electrical Engineering Handbook*, pages 721 – 736. Academic Press, Burlington, 2005.

[4] Juan Manuel Camacho and Victor Sosa. Alternative method to calculate the magnetic field of permanent magnets with azimuthal symmetry. *Revista mexicana de física E*, 59:8–17, 06 2013 Accessed 12/2020.

[5] Super Magnete. Physical magnet data, 2018 Accessed 11/2020. https://www.supermagnete.fr/eng/physical-magnet-data.

[6] R. Bayindir, I. Topaloğlu, and C. Ocak. Investigation of the effect of magnet thickness on motor losses of pm bldc machines using parametric approach method. In *2011 International Conference on Power Engineering, Energy and Electrical Drives*, pages 1–4, 2011 Accessed 12/2020.

[7] Chengyuan he and Thomas Wu Milwaukee. Permanent magnet brushless dc motor and mechanical structure design for the electric impact wrench system. *Energies*, 11:1360, 05 2018 Accessed 12/2020.

[8] Bikester. Current mid-motors, batteries an onboard computers, 2018 Accessed 12/2020. https://www.bikester.co.uk/over-ebikes/motors_batteries_displays.html.

[9] Electric Bike Review. Mid drive, internal gear reduction ratio and gear type., 2018 Accessed 12/2020. https://electricbikereview.com/forums/threads/mid-drive-internal-gear-reduction-ratio-and-gear-type.25854/.

[10] A. Cassat, Christophe Espanet, and N. Wavre. Bldc motor stator and rotor iron losses and thermal behavior based on lumped schemes and 3d fem analysis. pages 2469 – 2476 vol.4, 02 2002.

[11] Lin Peng. Statistical analysis of lithium-ion battery data collected on-board, 2013 Accessed 11/2020. https://www.diva-portal.org/smash/get/diva2:658429/FULLTEXT01.pdf.

[12] D. POWER. 18650 li-ion battery manufacturer and supplier, bulk order welcome., 2020 Accessed 11/2020. https://www.dnkpower.com/li-ion-18650-battery.

[13] D. POWER. Lithium ion battery manufacturer and supplier in china-dnk power, 2020 Accessed 11/2020. https://www.dnkpower.com/teslas-mass-production-21700-battery.

[14] Quang Dinh Pedro Ascencio James Marco Cheng Zhang*, Walid Allafi. Online estimation of battery equivalent circuit model parameters and state of charge using decoupled least squares technique, 2017 Accessed 11/2020. https://www.sciencedirect.com/science/article/pii/S0360544217317127.

[15] Christopher Arcus. Tesla model 3 chevy bolt battery packs examined, 2020 Accessed 11/2020. https://cleantechnica.com/2018/07/08/tesla-model-3-chevy-bolt-battery-packs-examined/.

[16] P. Van Den Bossche T. Turcksin and Universitée libre de Bruxelles P. Hendrick, Vrije Universiteit Brussel. Battery weight optimization for hovering aircraft, 20197 Accessed 11/2020. https://www.eucass.eu/component/docindexer/?task=download&id=5539.

[17] University of Wisconsin-Milwaukee Rohit Anil Ugle. Performance optimization of onboard lithium ion batteries for electric vehicles, May,2017 Accessed 11/2020. https://dc.uwm.edu/cgi/viewcontent.cgi?article=2552&context=etd/.

[18] Spinningmagnets. Introduction to battery pack design and building, part-1., 2019 Accessed 11/2020. https://www.electricbike.com/introduction-battery-design-1/.

[19] Luna Cycle. 18650 cell breakdown, June, 2015 Accessed 11/2020. https://lunacycle.com/blog/18650-cell-ebikes/.

[20] Paolo Salvagione. Science of cycling: Bicycle frame design — exploratorium, 2014 Accessed 11/2020. https://www.exploratorium.edu/cycling/frames4.html/.

[21] Corporate Finance Institute. Bagging (bootstrap aggregation) - overview, how it works, advantages, 2015 Accessed 11/2020. https://corporatefinanceinstitute.com/resources/knowledge/other/bagging-bootstrap-aggregation/.

[22] Mathwork. Choosing the algorithm, 2020 Accessed 11/2020. https://www.mathworks.com/help/optim/ug/choosing-the-algorithm.html#btr9d6u.

[23] Milos Manic Terence Soule. A distance measure comparison to improve crowding in multi-modal optimization problems, Sept, 2020 Accessed 11/2020. https://www.researchgate.net/publication/224182930_A_distance_measure_comparison_to_improve_crowding_in_multi-modal_optimization_problems.

[24] Relja. Bicycle drive chain standard dimensions, 2018 Accessed 12/2020. https://bike.bikegremlin.com/3555/bicycle-drive-chain-dimension-standards/.

[25] Engineering ToolBox. Metals and alloys - densities, 2004 Accessed 12/2020. https://www.engineeringtoolbox.com/metal-alloys-densities-d_50.html.

[26] Karl Stoerzinger. Shimano deore xt fh-m8110-b 148mm rear hub, 2019 Accessed 12/2020. https://www.kstoerz.com/freespoke/hub/534.

[27] QBP Tech. Chainrings: Understanding bcd, 2020 Accessed 12/2020. https://www.qbp.com/diagrams/tech_content/crank/bcd.html.

[28] Xiaojun Zhao, Yutong Du, Yang Liu, Zhenbin Du, Dongwei Yuan, and Lanrong Liu. Magnetostrictive properties of the grain-oriented silicon steel sheet under dc-biased and multisinusoidal magnetizations. *Materials*, 12:2156, 07 2019 Accessed 12/2020.

[29] H C. The properties of copper. *Nature*, 102:53–54, 1918 Accessed 12/2020.

[30] Micah. How much power does an electric bicycle need? *EbikeSchool*, 2018 Accessed 12/2020. http://www.ebikeschool.com/much-power-electric-bicycle-need/.

[31] MWS Wire Industries. Copper magnet wire data, 2016 Accessed 12/2020. https://mwswire.com/wp-content/uploads/2016/10/Copper-Magnet-Wire-Data.pdf.

[32] BPF. Acrylonitrile butadiene styrene (abs) and other specialist styrenics, 2020 Accessed 11/2020. https://www.bpf.co.uk/plastipedia/polymers/ABS_and_Other_Specialist_Styrenics.aspx.

[33] MakeitFrom. 6060 (almgsi, 3.3206, a96060) aluminum, 2009 Accessed 11/2020. https://www.makeitfrom.com/material-properties/6060-AlMgSi-3.3206-A96060-Aluminum/.